Robust UOWC systems against bubble-induced impairments via transmit/receive diversities [Invited]

Lian-Kuan Chen (陈亮光), Yingjie Shao (邵英婕)*, and Rui Deng (邓 锐)

Department of Information Engineering, The Chinese University of Hong Kong, Hong Kong, China
**Corresponding author: sy017@ie.cuhk.edu.hk*

Received July 29, 2019; accepted September 10, 2019; posted online October 10, 2019

We systematically investigate the bubble-induced performance degradation for underwater optical wireless communication (UOWC) with different bubble sizes and positions. By using different transmit and receive diversities, we investigate the effectiveness of spatial diversity on the mitigation of the bubble-induced impairment to the UOWC link. With the help of a 2 × 2 multiple input multiple output using repetition coding and maximum ratio combining, a robust 780 Mbit/s UOWC transmission is achieved. The corresponding outage probability can be significantly reduced from 34.6% for the system without diversity to less than 1%.

OCIS codes: 060.2605, 060.4510, 010.4455.
doi: 10.3788/COL201917.100006.

To explore the much-unexcavated resources in the ocean, human underwater activities have been intensified. With the advent of advanced underwater remotely operated vehicles (UROVs) and robots, ocean exploration has become more feasible and accessible. Real-time monitoring videos from remote sensors can provide timely and valuable information, which necessitates high-speed underwater wireless communications. To realize reliable communication between the UROV and the control center onshore[1], there are various solutions, such as undersea cables transport, acoustic communication, and underwater optical wireless communication (UOWC). The latter two wireless schemes provide great flexibility, whereas the acoustic communication exhibits long-range transmission capability, despite its much lower data rates. For UOWC, the transmissions at a data rate of gigabit per second using visible light in the green to blue region have been demonstrated[2–4], and real-time systems[5,6] and field-trial experiments[7,8] are also reported, thus receiving much attention recently. Nevertheless, the practical realization of UOWC is challenging in the undersea environment. One of the challenging factors is the bubble-induced impediment to the UOWC link. Multiple causes, including atmospheric, benthic, and cavitation, would incur the formation of bubbles[9], as illustrated in Fig. 1. The primary sources of bubbles in the upper ocean are breaking waves, rains impacting on the sea surface, as well as man's activities such as that from ship propellers. For benthic sources of bubbles, the biological activities and the vents and seeps of gases escaping from the seafloor are a possible cause to the generation of bubbles up to several millimeters in diameter. In Ref. [10], an experiment with the emulated bubble effect has been conducted in a single-link UOWC system. It is demonstrated that bubbles can incur discontinuous blocking for the light signal, and the corresponding UOWC transmission performance would be degraded seriously. Hence, the mitigation of the bubble effect is an important issue for a practical UOWC system. A statistical analysis of fading for UOWC in the presence of air bubbles has been reported in Ref. [11]. However, both studies mainly focus on received optical signal power distribution and lack a comprehensive study on the link performance, such as bit error rate (BER) and outage probability.

Optical multiple input multiple output (MIMO) utilizing spatial multiplexing has been widely investigated to enhance the capacity of the VLC system[12,13], as well as in indoor visible light communication (VLC) systems with line-of-sight (LOS) drawback[14]. In Ref. [15], a precoding scheme is proposed under a dynamic mobile receiver (RX) for an orthogonal frequency-division multiplexing (OFDM) optical wireless communication (OWC) system. An adaptive scheme is developed in Ref. [16], which can increase the overall performance of the VLC system, but also enhance the robustness of the system with blocking by an object within the transmission area. However, the effect of bubbles in the UOWC system is beyond a simple blocking or constant attenuation effect. The difference is that the bubbles are distributed discretely and dynamically in different sizes, and the light can be reflected and refracted by the moving bubbles. The contribution of this paper is a comprehensive study of the optical transmission impairment by various bubble effects and the investigation of the robustness of the UOWC link by transmit and receive diversity.

In this paper, firstly, we experimentally investigate the bubble-induced impairment for UOWC. The link performance in terms of BERs under different bubble sizes and relative location with respect to the transmitter (TX) is investigated and analyzed. Secondly, we investigate the effectiveness of spatial diversity using the MIMO technique to increase the link robustness. With the help of a 2 × 2 MIMO system using repetition coding (RC) and maximum ratio combining (MRC), a 780 Mbit/s UOWC

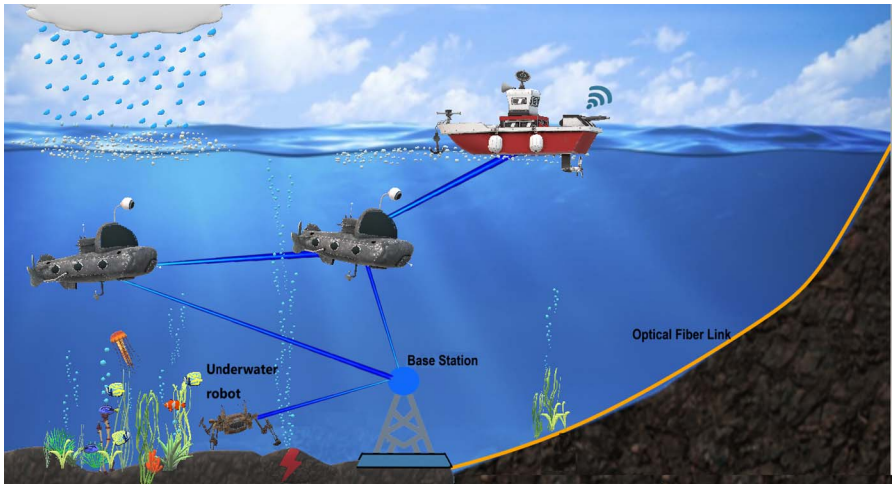

Fig. 1. Illustration of the ocean bubbles, UOWC links, and underwater communication networks.

system is demonstrated with a link outage probability of less than 1%, significantly decreased from 34.6%, for an optical link affected by bubbles.

Spatial diversity has been widely used in radio-frequency (RF) wireless transmission by utilizing multiple spatially distributed antennas to mitigate the Rayleigh fading in the wireless channel[17]. There are different formats according to different system configurations: single input multiple output (SIMO), multiple input single output (MISO), and MIMO. On the one hand, to exploit the transmit diversity (the MISO case), different space–time coding approaches can be employed, including RC and Alamouti-coded space–time block coding[18–20]. Here, we choose a low-complexity and effective scheme, the RC scheme, which can provide constructive power enhancement for an intensity modulation/direct detection (IM/DD) system.

On the other hand, to exploit receive diversity (the SIMO case), signals combination methods that include equal-gain combining (EGC), selective combining (SC), and MRC[21] are commonly used. The MRC is based on accurate channel state information at the RX side, thus exhibiting the optimal signal-to-noise ratio (SNR) performance among the linear diversity combination approaches. It sums up the multiple received signals with optimal combining ratios that are proportional to the received signal strength, assuming the local noises are independent with equal power. The combined signal can be expressed as

$$y = \sum_{i=1}^{N} h_i^* r_i = \sum_{i=1}^{N} h_i^* (h_i x + n_i) = \sum_{i=1}^{N} |h_i|^2 x + \sum_{i=1}^{N} h_i^* n_i, \tag{1}$$

where N is the total number of RXs, and h_i is the channel coefficient of the ith link. r_i is the received signal of ith RX, and it is composed of the transmitted signal x and noise term n_i. With MRC applied, the corresponding optimal SNR is given by

$$\mathrm{SNR} = \frac{E\left[\left(\sum_{i=1}^{N} |h_i|^2 x\right)^2\right]}{E\left[\left(\sum_{i=1}^{N} h_i^* n_i\right)^2\right]} = \frac{S \cdot \sum_{i=1}^{N} |h_i|^2}{N_0}. \tag{2}$$

Figure 2 shows the experimental setup and the digital signal processor (DSP) block for investigating the UOWC performance in the presence of air bubbles. Two TXs and

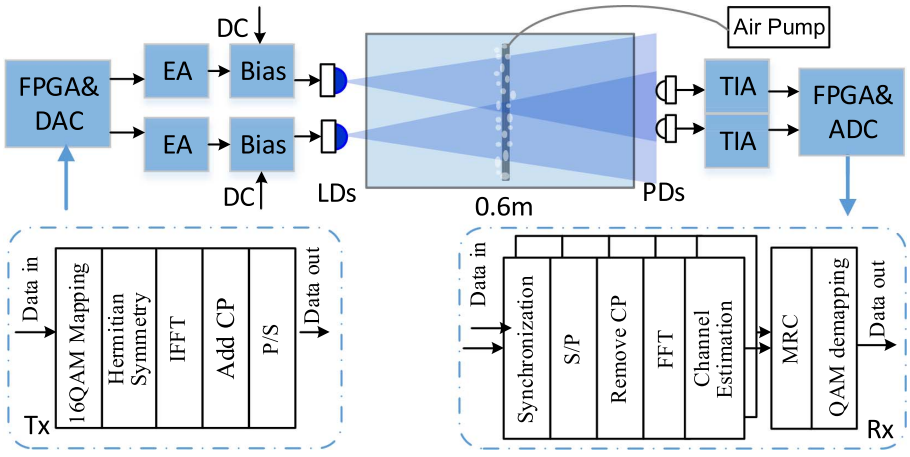

Fig. 2. Experimental setup and DSP block.

two RXs are used in the experiment to realize various spatial diversity schemes. The spaces between two TXs and two RXs are 10 cm and 8 cm, respectively. For the two TX lanes, the original electrical signals are generated by a field-programmable gate array (FPGA) board equipped with a dual-channel digital-to-analog converter (DAC) operating at 1 GS/s sampling rate with a 16-bit acquisition accuracy. The FPGA board is used to interact with a personal computer (PC) in real-time to receive the digital signal from the PC and to control the DAC to generate the corresponding electrical signals. The data is first mapped to 16-quadrature amplitude modulation (16-QAM) signals and then modulated as real-valued OFDM signals. The size of the inverse fast Fourier transform (IFFT) is 512, and out of which, 103 are modulated with data. This corresponds to a signal bandwidth of 200 MHz, which is chosen based on the RX bandwidth limitation. Taking the cyclic prefix (CP) length of 1/32 into consideration, the total data rate is 780 Mbit/s.

As the intensity of the generated signals is limited within a $1\,V_{\mathrm{pp}}$ dynamic range, the drive strength of the signals is inadequate. Hence, two amplifiers are used to amplify the signals before they are injected into the TX-side light sources. The light sources used in the experiment are blue laser diodes (LDs) (OSRAM PL450), with a center wavelength of 450 nm, within the open spectrum window for underwater transmission. Two bias-tees are used to combine a DC component and the amplified signals to drive the LDs. The amplification gain and the bias voltage are optimized at 9 dB and 5.4 V, respectively. Note that the maximum power of the LDs is 80 mW in the experiment. A water tank of the size 60 cm × 30 cm × 40 cm filled with tap water is used in the experiment for emulating the underwater channel. Bubbles are added in the channel by an air pump connected to different bubble dispensers for generating bubbles of different sizes. The total transmission link is short, ∼80 cm, as the study is mainly focusing on the bubble effects, and no lens is used. The spot size at the RX of one TX is around 35 cm × 15 cm.

At the RX side, two photodiodes (PDs, Hamamatsu S10784) equipped with trans-impedance amplifiers (TIAs) are used to realize an optical-to-electrical conversion to recover the received optical signals. The photosensitive area of the PD has a diameter of 3.0 mm. A dual-channel analog-to-digital converter (ADC) carried by the same FPGA receives the two-lane electrical signals. After uploading the captured data into the PC, an analysis is performed to evaluate the transmission performance under the bubble effect with and without spatial diversity.

In addition to the investigation of different spatial schemes, the transmission performance versus bubble sizes and positions is also investigated experimentally. To study the effect of air bubble size, we use a bubble dispenser with different hole sizes on it, while the flow rate of the air pump is fixed at 2 L/m throughout the experiment. In this way, with the same total air volume used, different bubble clusters can be obtained. Three sizes of bubbles are generated and investigated in this experiment, as shown in Figs. 3(b)–3(d). As estimated from the captured photos, they are categorized as large-, medium-, and small-size bubbles, with an approximate average size of 15 mm^2, 6 mm^2, and 2 mm^2, respectively. Meanwhile, we put the bubble tube at three different positions in the water tank to further investigate the system performance. The three positions are (i) near the TX (P1: 10 cm), (ii) approximately in the middle of the TX and the RX (P2: 40 cm), and (iii) near the RX (P3: 70 cm).

We first investigate the SNR and BER performance without bubbles, which is to be used as a reference for further evaluation of the link performance. Four schemes are used for comparison, i.e., single input single output (SISO) (1 × 1), SIMO (1 × 2), MISO (2 × 1), and MIMO (2 × 2). The received optical power for the two RXs is −3.2 dBm and −2.8 dBm (with one LD), respectively, For the two-LD case, the received power is increased to −0.6 dBm and −0.4 dBm, respectively. Figure 4(a) shows the SNR of the four schemes. The power fading at high frequency is due to the limited bandwidth of the positive-intrinsic-negative (PIN) PD and the RX circuit. When the optical spot at the RX is much larger than the RX area, no matter whether two LDs (2 × 1) or two PDs (1 × 2) are used, the received optical power will be nearly doubled when compared to the SISO case, resulting in an average 2.5 dB SNR improvement. Figures 4(b) and 4(c) show the BER versus the bandwidth used and the BER distribution at a bandwidth of 200 MHz, respectively. For the four schemes, the average BER is 1.31×10^{-2}, 5.58×10^{-3}, 3.92×10^{-3}, and 1.42×10^{-3}, respectively.

We then experimentally investigate the BER performance under the effect of bubbles with three different bubble sizes and at three different positions. For each

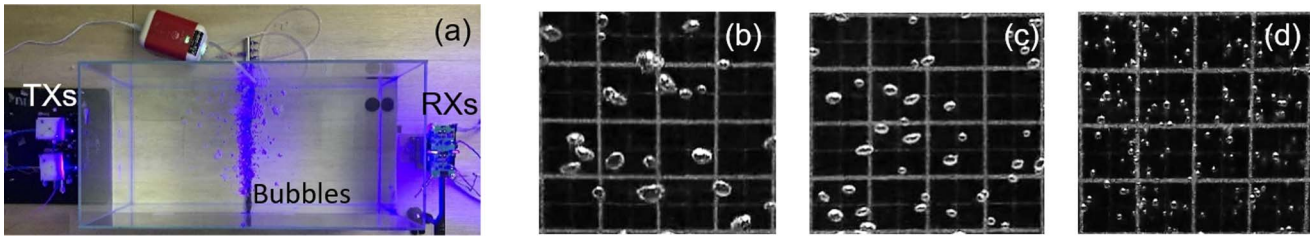

Fig. 3. (a) Experimental testbed. Images of bubbles captured in the experiment with an estimated average size of (b) large size: ∼15 mm^2, (c) medium size: ∼6 mm^2, (d) small size: ∼2 mm^2. Note that each square in the background is 10 mm × 10 mm.

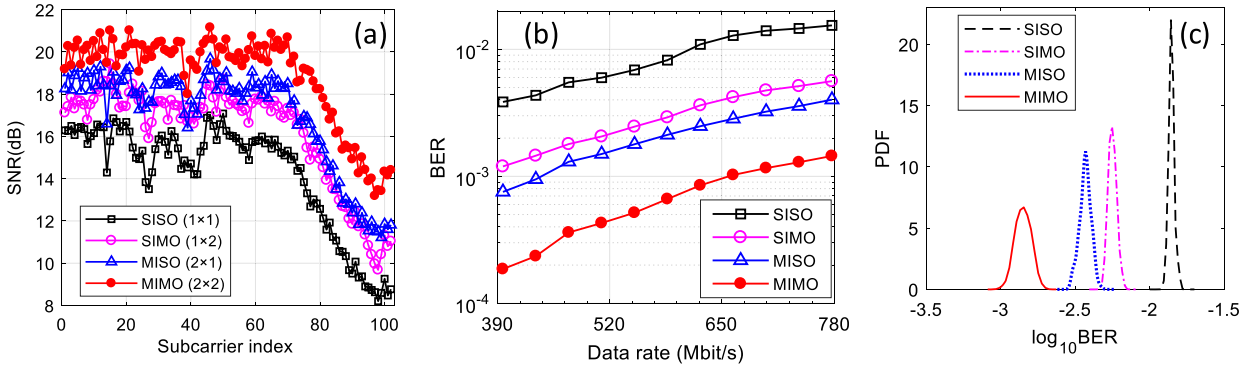

Fig. 4. Performance of UOWC system without bubbles: (a) SNR versus subcarrier index with a bandwidth of 200 MHz, (b) BER versus data rate (different bandwidth used), (c) the distribution of packet BER for 200 packets with a signal bandwidth of 200 MHz.

scheme, 500 packets are captured to analyze the bubble-induced impairment and the mitigation capability provided by spatial diversity. Each packet contains $\sim 1.2 \times 10^5$ bits to calculate BER. In each figure of Fig. 5, 200 samples are shown to illustrate the bubble-induced effect under different scenarios to capture the variations

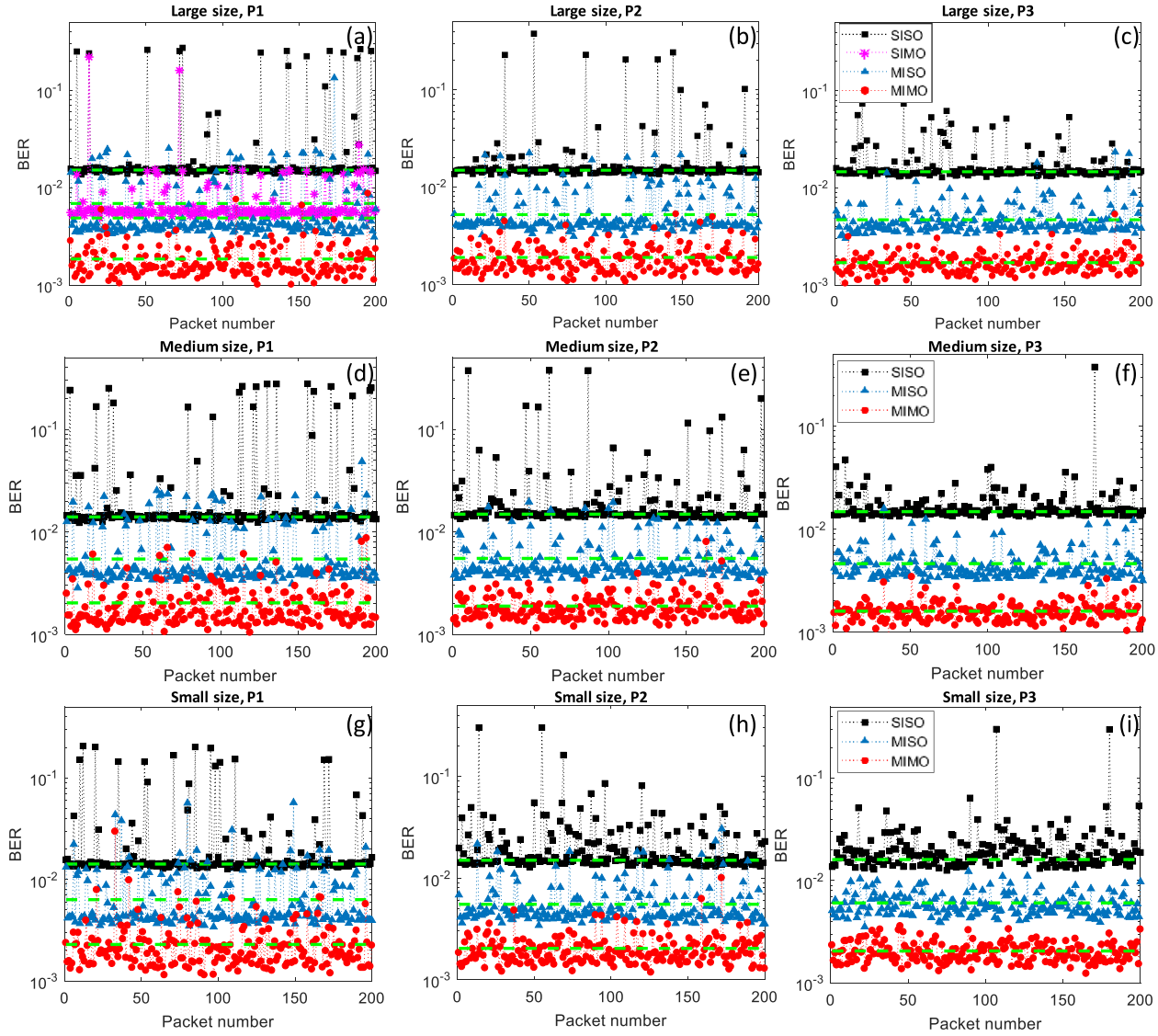

Fig. 5. BER performance of 200 packets with (a)–(c) large-size bubbles, (d)–(f) medium-size bubbles, and (g)–(i) small-size bubbles, at a distance from TXs of P1: 10 cm, P2: 40 cm, and P3: 70 cm, respectively. The green dash lines correspond to the mean levels of different schemes.

of BER due to the dynamic bubbles. Note that we only show the SIMO case in Fig. 5(a) and omit it in others to avoid the overlap with the MISO case. Similar performance is observed for both SIMO and MISO schemes. For the SISO scheme, it is clear that the bubble may block the LOS light path and cause severe performance degradation. As shown in Figs. 3(b) and 3(c), when the bubble size decreases, the number of bubbles increases. When the bubble size is smaller, the blocking effect is less significant, which may give rise to partial light detection at the RX. Therefore, as shown in Figs. 5(b), 5(e), 5(h), BER distribution undergoes from less frequent but larger variation to more frequent but smaller variation. Compared with the bubble size, the position of bubbles results in more distinct performance. With the bubble position moving away from the TX, the number of packets suffering severe fading reduces, and the remaining packets exhibit a larger BER variation. This is due to the light reflection and scattering with the bubbles. For MISO and SIMO schemes, by providing a diversity gain of two, the probability of deep fading decreases significantly compared with the SISO scheme.

The MIMO case (the red curves in Fig. 5), which further doubles the diversity gain, provides the most robust link as well as the lowest average BER. The performance is relatively constant with different bubble sizes at the same location. Next, we consider the effect of the bubble location. The BERs show a decreased variance when the bubble location moves away from the TXs. This also indicates a consistent trend that the complete blocking for each SISO link becomes less probable, and scattered light increases the possibility of receiving partial signals. The green dash lines show the average BER of the packets that are below soft-decision forward error correction (SD-FEC) limit (2×10^{-2}), which remains relatively constant for all the cases.

We then analyze the probability density function (PDF) of the BERs of 500 packets, as shown in Fig. 6. For all cases, the BER distribution spreads wider, compared with the cases without bubbles [Fig. 4(c)]. The SISO case shows the largest difference in PDF under various scenarios. For the small bubble case at position 3 (near the RX), the peak of the PDF distribution for SISO reduces significantly, indicating that the BER has a wider spread. In general, by exploiting the spatial diversity, the distribution for almost all scenarios remains relatively constant, which further verifies the observation from Fig. 5.

At last, we analyze the BER variance, packet loss rate (PLR), and the average BER of successfully received packets to further study the bubble-induced effect and to verify the diversity gain provided by different schemes. The BER variance in Table 1 further confirms the previous observation that the variance is larger when bubbles are closer to the TX. The PLRs are given in Table 2. Note that, for the loss packet number less than five, the PLR is denoted as <1%. For the SISO case, as the distance increases or the bubble size decreases, the PLR shows a rising trend, whereas, for the SIMO and MISO cases, the

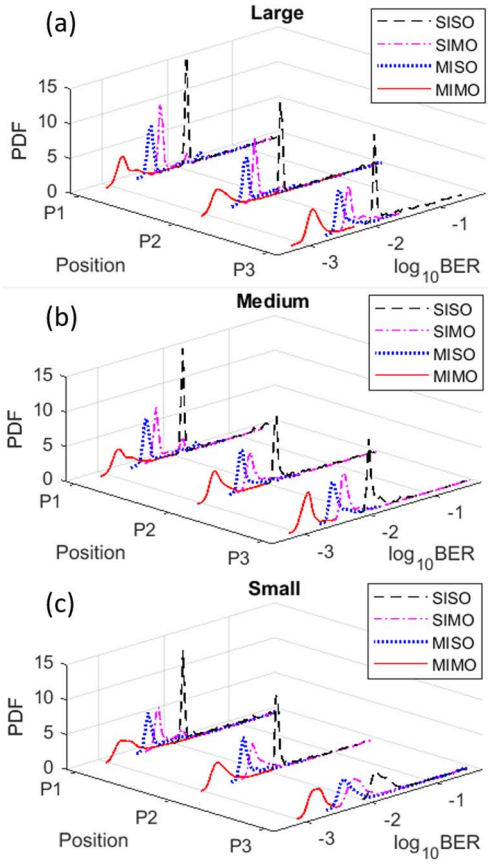

Fig. 6. PDFs of the BER performance under scenarios with different bubble sizes: (a) large, (b) medium, and (c) small.

PLR decreases. This is because the original performance of SISO is near the FEC limit and more frequent fluctuation in BER leads to more packets having BER above FEC limits. For the MIMO scheme, the outage probability is <1% for all the scenarios. By providing multiple independent light paths in the UOWC link, the MIMO scheme significantly reduces the BER fluctuation and increases the link robustness. The average BER is shown in Fig. 7.

Table 1. BER Variance

Size/Position		SISO	SIMO	MISO	MIMO
L	P1	2.83E-03	2.80E-04	2.09E-03	9.65E-07
	P2	2.63E-03	1.08E-04	6.46E-04	5.71E-07
	P3	8.55E-04	8.04E-06	5.61E-06	2.23E-07
M	P1	3.81E-03	1.42E-04	3.83E-04	1.33E-06
	P2	2.90E-03	8.14E-04	1.15E-05	4.49E-07
	P3	5.59E-04	5.45E-06	3.37E-06	1.46E-07
S	P1	2.25E-03	7.26E-04	3.03E-04	2.41E-06
	P2	1.40E-03	1.03E-04	1.22E-05	7.15E-07
	P3	7.02E-04	8.93E-05	2.63E-06	1.63E-07

Table 2. Packet Loss Rate

Size/Position		SISO	SIMO	MISO	MIMO
L	P1	13.0%	3.4%	9.6%	<1%
	P2	14.6%	1.6%	7.8%	<1%
	P3	20.4%	<1%	<1%	<1%
M	P1	16.4%	4.4%	5.6%	<1%
	P2	20.6%	5.2%	<1%	<1%
	P3	21.0%	<1%	<1%	<1%
S	P1	24.4%	3.2%	6.4%	<1%
	P2	17.0%	2.8%	2.0%	<1%
	P3	34.6%	2.4%	1.2%	<1%

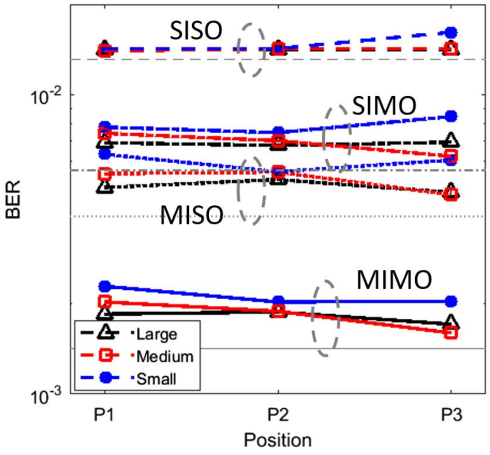

Fig. 7. Average BER of packets below SD-FEC. (The gray lines show the reference BER of each scheme without bubbles.)

The performance under the small bubble case exhibits the worst BER.

In summary, we experimentally investigate the performance under different bubble sizes and positions. The statistics of the PLR and BER through a UOWC channel with bubbles are analyzed. For the SISO scheme, the results show that as the distance to the TX side increases or the bubble size decreases, the less possibility of deep fading occurs. Without considering the lost packet, the average BER remains similar. Moreover, via spatial diversity, including the SIMO, MISO, and MIMO schemes, it significantly reduces the BER fluctuation and increases the link stability. A robust 780 Mbit/s 2×2 MIMO system is achieved under different scenarios of bubble size and position. Enhancement in both BER (reduced from 1.31×10^{-2} to 1.42×10^{-3}) and link reliability (outage probability reduced from the worst case of 34.6% to less than 1% for all cases) is achieved.

This work was supported in part by the HKSAR UGC/RGC grants (Nos. GRF 14215416 and GRF 14201217).

References

1. P. Jasiobedzki and R. Jakola, http://citeseerx.ist.psu.edu/viewdoc/download?doi=10.1.1.118.9489&rep=rep1&type=pdf (2007).
2. Y. Chen, M. Kong, T. Ali, J. Wang, R. Sarwar, J. Han, C. Guo, B. Sun, N. Deng, and J. Xu, Opt. Express **25**, 14760 (2017).
3. C. Shen, Y. Guo, H. M. Oubei, T. K. Ng, G. Liu, K. H. Park, K. T. Ho, M. S. Alouini, and B. S. Ooi, Opt. Express **24**, 25502 (2016).
4. T. C. Wu, Y. C. Chi, H. Y. Wang, C. T. Tsai, and G. R. Lin, Sci. Rep. **7**, 40480 (2017).
5. Y. Shao, R. Deng, J. He, K. Wu, and L. K. Chen, in *Proceedings of ECOC* (2019).
6. P. Wang, C. Li, and Z. Xu, J. Light. Technol. **36**, 2627 (2018).
7. G. Cossu, A. Sturniolo, A. Messa, S. Grechi, D. Costa, A. Bartolini, D. Scaradozzi, A. Caiti, and E. Ciaramella, J. Light. Technol. **36**, 5371 (2018).
8. T. Sawa, http://www.godac.jamstec.go.jp/catalog/data/doc_catalog/media/KR17-11_leg2_all.pdf (2017).
9. D. K. Woolf, *Encyclopedia of Ocean Sciences*, 2nd ed. (Elsevier, 2001), p. 352.
10. H. M. Oubei, R. T. ElAfandy, K. Park, T. K. Ng, M. Alouini, and B. S. Ooi, IEEE Photon. J. **9**, 7903009 (2017).
11. M. V. Jamali, A. Mirani, A. Parsay, B. Abolhassani, P. Nabavi, A. Chizari, P. Khorramshahi, S. Abdollahramezani, and J. A. Salehi, IEEE Trans. Commun. **66**, 4706 (2018).
12. Y. Hong, T. Wu, and L. K. Chen, IEEE Photon. Technol. Lett. **28**, 907 (2016).
13. Y. Hong, L. K. Chen, and J. Zhao, Opt. Express **27**, 12806 (2019).
14. K. Ying, H. Qian, R. J. Baxley, and S. Yao, IEEE J. Sel. Areas Commun. **33**, 1949 (2015).
15. Y. Hong and L. K. Chen, Opt. Lett. **41**, 3763 (2016).
16. P. Deng and M. Kavehrad, in *Proceedings of OFC* (2017), paper Th1E.5.
17. D. Tse and P. Viswanath, *Fundamentals of Wireless Communication* (Cambridge University, 2005).
18. S. M. Alamouti, IEEE J. Select. Areas Commun. **16**, 1451 (1998).
19. M. Safari and M. Uysal, IEEE Trans. Wireless Commun. **7**, 4445 (2008).
20. Y. Shao, Y. Hong, R. Deng, and L. K. Chen, in *Proceedings of OECC* (2019).
21. D. Brennan, Proc. IEEE **47**, 1075 (1959).